Dynamics of the Optical-Pumping Cycle of F Centers in Alkali Halides–Theory and Application to Detection of Electron-Spin and Electron-Nuclear-Double-Spin Resonance in the Relaxed-Excited State*

L. F. Mollenauer and S. Pan
Department of Physics, University of California, Berkeley, California 94720
(Received 14 February 1972)

The dynamics of the optical-pumping cycle of F centers in alkali halides are governed by two prime factors: the large magnetic circular dichroism exhibited by the F band and a large electron-spin memory over the entire cycle. A model of the pump cycle and associated rate equations are given. The most general solutions are given, and important special cases are treated in detail. A number of new experimental techniques are based on the special characteristics of the rate-equation solutions. Among these are purely optical techniques for measuring (i) the degree of spin memory in the entire pumping cycle and (ii) the spin-lattice relaxation rate in the relaxed-excited state (RES). But the most important new development based on the rate-equation solutions is the optical-trigger detection of both electron-spin resonance (ESR) and electron-nuclear–double-spin resonance of the RES. Results of these experiments, including ESR g factors and hyperfine splittings for the RES are given and discussed.

I. INTRODUCTION

The F-center absorption band in alkali halides exhibits a large magnetic circular dichroism (MCD),[1-3] which is paramagnetic in origin. Consequently, one can produce large, inverted, electron-spin polarizations by pumping with intense circularly polarized light.[1,3] The above facts have been known for quite some time, but it was not until recently that the dynamics of the optical-pumping cycle have been truly understood. In particular, the pump cycle exhibits a large electron-spin-memory effect, as first discovered by Schmid and Zimmerman,[4] and later and independently by ourselves.[5] This spin memory has had rather profound consequences for the experimental study of the relaxed-excited state (RES) of the F center. In the first place, one can take advantage of the spin memory to optically detect both electron spin resonance (ESR) and electron-nuclear–double-spin resonance (ENDOR), as we have demonstrated in a recent series of letters.[5,6] Thus, precise spectroscopic splitting factors (g factors) are now known for the F-center RES in a number of host lattices, and the ENDOR data promise to yield detailed information about the spatial distribution of the RES wave function. Hence, the long-standing question[7] of the "diffuse" vs "compact" nature of the RES may be given a definitive empirical answer in the near future. These resonance measurements are especially important in view of the fact that dichroic effects in the F-center luminescence are rather small,[8-10] and hence mitigate against a precise moments analysis; furthermore, the theoretical interpretation of such an analysis is usually rather ambiguous, i.e., it often depends strongly on the choice of a particular theoretical model. In the second place, Porret and Lüty have taken advantage of the spin memory to demonstrate spin dependence of the tunneling effect between excited F-center neighbors.[11] Finally, Ruedin *et al.* of the Neuchâtel group have very recently demonstrated[12] an alternative optical detection technique for the ESR of the F-center RES; their method is based on the Porret-Lüty effect.

After giving a brief phenomonological description of the MCD of the F absorption band (Sec. II), in Sec. III we write down the complete rate equations that govern the dynamics of the F-center optical-pumping cycle, and we display this solution for a large number of important special cases, as well as giving the most general solution. In Sec. IV we show how one may take advantage of the electron-spin memory in order to detect ESR in the RES, and we also give there the latest and best results for g factors and ESR linewidths. In Sec. V we give details of the extension of the ESR measurements to include ENDOR, and finally, in Sec. VI, we describe some recent and purely optical measurements of the spin-lattice relaxation rate in the RES. A theoretical model and complete discussion of the spin-memory effect itself is given in the paper that immediately follows this one.

II. MAGNETIC CIRCULAR DICHROISM OF OPTICAL-ABSORPTION BAND

The MCD of the optical-absorption band is fundamental to all of the experiments described in this paper. Therefore, in this section we give a brief phenomenological description of the MCD and of its measurement. This description will

serve both to fix ideas and to introduce certain important fundamental notation. A theoretical analysis of the MCD is delayed until the following paper.

The absorption is from a magnetic-doublet ground state ($^2S_{1/2}$) to a p-like band. The MCD is, by definition, differential absorption of right- and left-circularly polarized light into this band, where the light is propagating along the direction of an externally applied magnetic field H_0. Thus we are concerned here with the σ^+ and σ^- transitions of the Zeeman effect. For transmitted and incident intensities $I^\pm$ and $I_0^\pm$, respectively, of $\sigma^\pm$ light, we have the relation

$$I^\pm = I_0^\pm e^{-l\gamma(\sigma^\pm)} \quad , \tag{1}$$

where l is the crystal thickness and γ is the absorption coefficient per unit length. We choose to measure a MCD signal defined by

$$S = (I^+ - I^-)/(I^+ + I^-) \quad . \tag{2}$$

In practice, the dichroism signal is derived in the following way. The polarization of the light beam is modulated rapidly and symmetrically between σ^+ and σ^- before it impinges on the sample. Thus, if the modulation is sinusoidal, the incident intensities may be written as

$$I_0^\pm(t) = I_0[\tfrac{1}{2}(1 \pm \sin\omega t)] \quad , \tag{3}$$

where ω is the modulation frequency. The output of the photomultiplier then corresponds to the sum of the transmitted intensities:

$$I(t) = \tfrac{1}{2}(I^+ + I^-) + \tfrac{1}{2}(I^+ - I^-)\sin\omega t \quad . \tag{4}$$

By means of a feedback loop[3] which operates on the photomultiplier-tube supply voltage (and hence has control of the multiplier gain), the photomultiplier output corresponding to the first term in Eq. (4) is held fixed at unity. The amplitude of the second term is measured with the aid of a lock-in detector. Thus, in effect, the output of the lock-in is just the normalized signal defined by Eq. (2).

The ground-state electron-spin polarization P is defined by

$$P = (n_+ - n_-)/(n_+ + n_-) \quad , \tag{5}$$

where n_+ and n_- are the populations of the $M_s = +\frac{1}{2}$ and $M_s = -\frac{1}{2}$ states, respectively. Note that by definition, Eq. (5), P is *negative* for a thermal-equilibrium population distribution. In terms of its dependence on P, it is well known[2] that the MCD signal S can be divided into two components:

$$S = S_p(P) + S_d(H_0) \quad , \tag{6}$$

where S_p, the paramagnetic contribution, is directly proportional to P; whereas S_d, the diamagnetic term, which arises from (unresolved) Zeeman splittings in the excited state, is independent of P, and is strictly proportional to H_0. For $|P| \cong 1$, S_p is by far the larger term, and furthermore, this paramagnetic term is the one that is so very useful in the optical-pumping experiments.

The above-mentioned division of the MCD signal into two terms arises from the simple fact that the absorption coefficient $\gamma(\sigma^\pm)$ may be written as a simple sum: $\gamma(\sigma^\pm) = \gamma_p(\sigma^\pm) + \gamma_d(\sigma^\pm)$, where the subscripts p and d again refer to paramagnetic and diamagnetic parts. To facilitate analysis of S_p in terms of ground-state populations, one may write further

$$\gamma_p(\sigma^\pm) = \phi^+ \alpha(\sigma^\pm, +) + \phi^- \alpha(\sigma^\pm, -) \quad ,$$

where $\alpha(\sigma^\pm, +)$ and ϕ^+ are the fractional absorption coefficient and fractional population for the ground-state sublevel $M_s = +\frac{1}{2}$, and $\alpha(\sigma^\pm, -)$ and ϕ^- are the corresponding quantities for $M_s = -\frac{1}{2}$. From the fact that the ground state is a Kramers doublet, the absorption from that state must obey the symmetry $\alpha(\sigma^+, +) = \alpha(\sigma^-, -) \equiv \alpha^+$ and $\alpha(\sigma^+, -) = \alpha(\sigma^-, +) \equiv \alpha^-$. Under the assumption that $l[\gamma(\sigma^+) - \gamma(\sigma^-)] \ll 1$, it can be shown that

$$S_p(\omega_l) = l\gamma_0(\omega_l) f_p(\omega_l) P \quad , \tag{7}$$

where ω_l is the light frequency, γ_0 is the absorption coefficient for $H_0 = 0$, and where f_p, the dichroic fraction associated with S_p, is defined as

$$f_p = \frac{\alpha^+ - \alpha^-}{\alpha^+ + \alpha^-} \quad . \tag{8}$$

According to Eq. (7), $S_p(\omega_l)$ is a direct measure of $\gamma_0 f_p$ for a fixed temperature and fixed field H_0. Figure 1 shows $S(\omega_l)$ for the F absorption band in the three host lattices KCl, KBr, and KI, for $T = 1.6\,^\circ$K and for $H_0 \sim 20$ kOe. Note that there are two points in the band, more or less symmetrically spaced with respect to the band center, for which $|S|$ is a maximum. For convenient future reference, we define f_p^0 to be the maximum absolute value of f_p for $P = -1$ (corresponding to thermal equilibrium at zero temperature). These very broad maxima in $|f_p|$ begin just outside the $|S|$ maxima.

The experiments take advantage of the MCD in two fundamental ways. First, a polarization-modulated light beam, whose frequency corresponds to one or the other of the dichroic peaks, provides a convenient and sensitive way of monitoring P. According to Eq. (7), the signal is linear in P, and it can be calibrated by making reference to a thermal-equilibrium polarization. Because of the large oscillator strength of the F absorption band, and because of the fact that f_p^0 is large, in practice one can detect $\Delta P \gtrsim 0.01\%$ in a 1-mm-thick crystal containing only 10^{16} F centers/cm^3. The MCD monitor thus serves as a convenient and precise way to measure the effects of optical pumping on

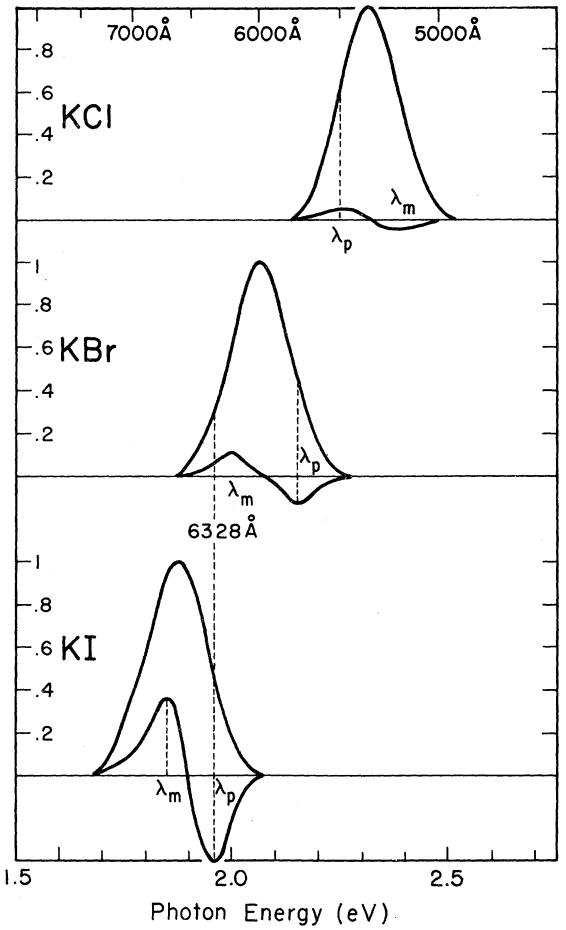

FIG. 1. MCD signals S (smaller derivativelike curves) for the F absorption band in the three host lattices KCl, KBr, and KI, for $T=1.6\,^{\circ}\mathrm{K}$ and $H_0 \sim 20$ kOe. Calculated Gaussians that approximate the direct absorption have been included for comparison. The vertical scale gives S as an absolute fraction, for crystals whose optical depth ($\gamma_0 l$) is of order unity at either of the peaks of $|S|$. λ_p and λ_m refer to pump and monitor wavelengths used in the experiments (see text).

the electron spins and as a very sensitive and convenient detector in all resonance experiments.

Second, but of equal importance, P can be manipulated over a wide range, including large inverted polarizations, by pumping with intense σ^+ or σ^- light. That is, if u_+ and u_- stand for the pump rates out of the $M_s=+\frac{1}{2}$ and $M_s=-\frac{1}{2}$ substates, respectively, then for pumping at a dichroic peak, the fractional differential pump rate will be

$$(u_- - u_+)/(u_- + u_+) = \pm f_p^0 \ , \tag{9}$$

the sign depending on choice of dichroic peak and pump polarization. If there is some degree of spin mixing on the return to the ground state, if there is no significant degree of thermalization as the system passes through intermediate states, and if the pumping effect is fast enough to overwhelm spin-lattice relaxation in the ground state, then one obtains

$$P_s = \pm f_p^0 \ , \tag{10}$$

where P_s is the value for a saturated pumping effect. A careful examination of all aspects of the optical-pumping cycle and its associated rate equations is the subject of the next section.

III. DYNAMICS OF OPTICAL-PUMPING CYCLE

A. Description of Optical-Pumping Cycle

The optical-pumping cycle consists of four processes: (i) absorption of a photon and excitation into the absorption band; (ii) nonradiative decay into the RES (relaxed-excited state); (iii) luminescence from the RES to the unrelaxed ground state, and (iv) nonradiative decay back into the normal (relaxed) ground state. These processes are illustrated schematically in Fig. 2.

Although there exists a basis of at least eight electronic states (2—2s and 6—2p) from which the various sublevels of the RES may be formed, for the purpose of describing the optical-pumping cycle, one need be concerned only with the lowest-lying magnetic doublet from which the luminescence occurs. Furthermore, it is well known that the luminescence from the RES occurs with essentially 100% quantum efficiency,[13] for $T \lesssim 50\,^{\circ}\mathrm{K}$, and for sufficiently low F-center concentrations. (If the F-center concentration is high enough, say 10^{17} /cm^3 or greater, the tunneling processes described by Porret and Lüty will significantly reduce the quantum efficiency.) In this paper we

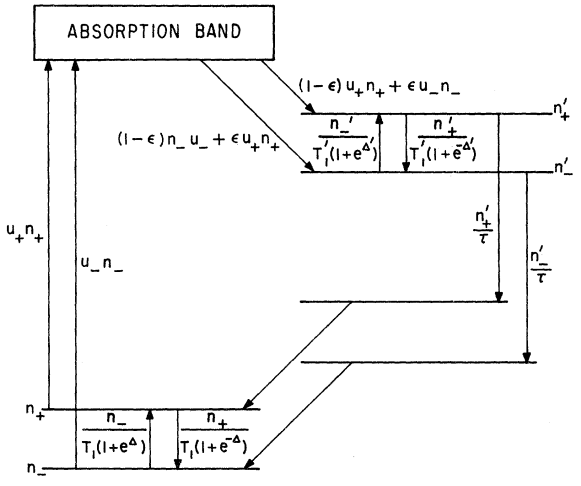

FIG. 2. Energy levels and transition rates for the optical-pumping cycle of the F center. Magnetic sublevels of the ground state are at the lower left; magnetic sublevels of the RES are at the upper right-hand side (see text).

will be concerned primarily with the system behavior at liquid-He temperatures, and for low F-center concentrations. Therefore, our assumption of 100% quantum efficiency will usually be a good one.

The spin memory of the pumping cycle is best described through introduction of the spin-mixing parameter ϵ, where ϵ is defined to be that fraction of spins that are flipped in a single pump cycle. One may further analyze ϵ according to the contributions made to it by each of the above-mentioned processes. Thus, let ϵ_1 designate the degree of spin mixing in the absorption-band states, ϵ_2 the contribution of the nonradiative decay into the RES, ϵ_3 the degree of spin mixing in the RES, and ϵ_4 the contribution of the second nonradiative-decay process. If none of the above processes reverse each other, then ϵ should be related to its components by the equation

$$(1-\epsilon)=(1-\epsilon_1)(1-\epsilon_2)(1-\epsilon_3)(1-\epsilon_4)\ , \qquad (11a)$$

or, since ϵ is usually $\ll 1$,

$$\epsilon \cong \epsilon_1+\epsilon_2+\epsilon_3+\epsilon_4\ . \qquad (11b)$$

At least ϵ_4 ought to be very small relative to the other contributions to ϵ. That is, the second nonradiative decay involves electronic states of zero orbital momentum, with the consequence that there is no effective spin-phonon coupling mechanism. Furthermore, there is good reason to believe that the magnetic sublevels of the RES have nearly pure spin character, so that ϵ_3 is also probably small relative to the sum $\epsilon_1+\epsilon_2$. Therefore, in the following rate equations, ϵ will be substituted for the sum $\epsilon_1+\epsilon_2$, and ϵ_3 and ϵ_4 will be neglected entirely. This substitution greatly simplifies the form of the rate equations, without at the same time seriously altering the nature of the solutions. For example, the exact expression for the spin-flipping rate due to optical pumping involves the term $\epsilon-2(\epsilon_1+\epsilon_2)(\epsilon_3+\epsilon_4)$, whereas in the approximation we present here, the corresponding term is just ϵ. [See Eq. (15) in Sec. III B]. Note that the two terms are not sensibly different, even if $\epsilon_3+\epsilon_4$ is *not* small relative to $\epsilon_1+\epsilon_2$, as long as $\epsilon \ll 1$. Thus, these approximations ought to be nearly exact for KCl and KBr, where $\epsilon \lesssim 5\%$. On the other hand, for KI, where $\epsilon \cong 24\%$, their effects might be discernable in the most precise work.

B. Rate Equations

The rate equations that govern the dynamics of optical pumping are as follows:

$$\frac{dn_+}{dt}=-u_+n_+ +\frac{n'_+}{\tau}-\frac{1}{T_1}\left(n_+-\frac{n_++n_-}{1+e^{\Delta}}\right)\ , \qquad (12a)$$

$$\frac{dn_-}{dt}=-u_-n_- +\frac{n'_-}{\tau}-\frac{1}{T_1}\left(n_--\frac{n_++n_-}{1+e^{-\Delta}}\right)\ , \qquad (12b)$$

$$\frac{dn'_+}{dt}=(1-\epsilon)u_+n_+ +\epsilon u_-n_- -\frac{n'_+}{\tau} -\frac{1}{T'_1}\left(n'_+-\frac{n'_++n'_-}{1+e^{\Delta'}}\right), \qquad (12c)$$

$$\frac{dn'_-}{dt}=(1-\epsilon)u_-n_- +\epsilon u_+n_+ -\frac{n'_-}{\tau} -\frac{1}{T'_1}\left(n'_--\frac{n'_++n'_-}{1+e^{-\Delta'}}\right), \qquad (12d)$$

where n_+ and n_- are the populations of the ground-state sublevels $M_s=+\frac{1}{2}$ and $M_s=-\frac{1}{2}$, T_1 is the ground-state spin-lattice relaxation time, and $\Delta=g\mu_B H_0/kT$, where g is the spectroscopic splitting factor for the ground state, μ_B the Bohr magneton, k is Boltzmann's constant, and T is the absolute temperature; the corresponding quantities for the RES are indicated by primes; u_+ and u_- have the same meaning as in Eq. (9), and τ is the optical decay time of the luminescence from the RES.

With the aid of the substitutions $N=n_++n_-$, $n=n_+-n_-$, $N'=n'_++n'_-$ and $n'=n'_+-n'_-$, Eqs. (12) can be put in a form more tractable of solution:

$$\frac{dN}{dt}=-\frac{N}{2}(u_++u_-)+\frac{n}{2}(u_--u_+)+\frac{N'}{\tau}\ , \qquad (13a)$$

$$\frac{dn}{dt}=\left(\frac{1}{2}(u_--u_+)-\frac{1}{T_1}\tanh\tfrac{1}{2}\Delta\right)N -\left(\frac{1}{2}(u_++u_-)+\frac{1}{T_1}\right)n+\frac{n'}{\tau}\ , \qquad (13b)$$

$$\frac{dn'}{dt}=\tfrac{1}{2}(1-2\epsilon)[(u_++u_-)n-(u_--u_+)N] -\frac{n'}{\tau}-\left(\frac{1}{T'_1}\right)(\tanh\tfrac{1}{2}\Delta')N'-\left(\frac{1}{T'_1}\right)n'\ , \qquad (13c)$$

$$\frac{dN'}{dt}=-\frac{dN}{dt}\ . \qquad (13d)$$

The two nonradiative-decay processes are thought to take place very rapidly ($\sim 10^{-11}$ sec); since this time is very short relative to τ($\tau\sim 10^{-6}$ sec), it is quite reasonable to neglect the time-average populations in the two unrelaxed states. Furthermore, for the usual pump sources $(u_++u_-)\tau \lesssim 10^{-3}$ or 10^{-4}; thus dN/dt can be essentially neglected. That is, on a time-average basis, most of the F centers are in the ground state. Finally, it should be noticed that the rate equations take account of spin-lattice relaxation in the RES as well as in the ground state. On the other hand, there is considerable evidence that the effects of spin-lattice relaxation in the RES are negligible, at least for very low temperature ($T\sim 1.6\,^\circ$K) and for modest fields H_0. Therefore, it is realistic and instructive to examine the solutions in the simpler case where

$\tau/T_1' = 0$, before looking at the most general solution.

C. Solution for Transient Behavior; Measurement of ϵ When $\tau/T_1' = 0$

In an experiment where a pump light is turned on suddenly at time $t = 0$, the ground-state polarization P behaves as follows:

$$P(t) = P_f + (P_i - P_f)\, e^{-\tau/T_r} \quad , \tag{14}$$

where P_i and P_f are the initial and final polarizations, respectively, and where the rise time T_r is given by

$$1/T_r = 1/T_1 + \epsilon(u_+ + u_-) \quad . \tag{15a}$$

For convenient future reference, we define

$$1/T_p = \epsilon(u_+ + u_-) \quad . \tag{15b}$$

The most reliable method for measuring ϵ is based upon Eq. (15a). That is, the exponential rise of P can be monitored by a weak, modulated light beam tuned to one dichroism peak [as indicated by Eq. (7)], while the pump beam is tuned to the other peak. Thus, T_r can be measured directly and very conveniently. Since T_1 is already known (furthermore, it is usually possible to have $1/T_r \gg 1/T_1$), and since $u_+ + u_-$ can be calculated from a measurement of the absolute pump-light intensity, ϵ can be inferred from Eq. (15a). The best results to date of such measurements are as follows: for KCl, $\epsilon = 0.01$; for KBr, $\epsilon = 0.04$, and for KI, $\epsilon = 0.24$. These measurements were made at $T = 1.6\,^{\circ}\mathrm{K}$ and over a wide range of magnetic field values and pump-light intensities; the results were always essentially independent of such variations. Because of difficulties in the measurement of the pump intensity, the ϵ values quoted above are not accurate to better than about $\pm 25\%$.

D. Steady-State Solution for Pumping with Fixed Polarization ($\tau/T_1' = 0$)

The ground-state polarization is given by

$$P = \frac{P_s - (T_p/T_1)\tanh\frac{1}{2}\Delta}{1 + T_p/T_1} \quad , \tag{16}$$

where the value for P_s is given by Eq. (10) for pumping with σ^+ or σ^- light, and where $P_s = 0$ for pumping with linearly polarized light. Polarization in the RES, P', is given by

$$P' = \frac{-(1-2\epsilon)[(u_- - u_+) + (u_- + u_+)\tanh\frac{1}{2}\Delta]}{[(u_+ + u_-) + (u_- - u_+)\tanh\frac{1}{2}\Delta] + 4\epsilon u_+ u_- T_1} \quad . \tag{17}$$

Equation (17) has interesting behavior at two limiting extremes. The first occurs for very weak pumping with linearly polarized light, i.e., where $u_- = u_+$ and where $2\epsilon u T_1 \ll 1$. Then one obtains simply $P' \cong (1-2\epsilon)P$; that is, the ground-state polarization is transferred to the RES, diminished only by the factor $(1-2\epsilon)$. The second case occurs for strong pumping with light of *any* steady polarization (σ^+, σ^- or linear). That is, when $2\epsilon u T_1 \gg 1$, $P' \sim (2\epsilon u T_1)^{-1} \to 0$ as $u \to \infty$.[14] Furthermore, since $N' \sim N u \tau$, the number of excess spins available to produce a standard ESR absorption, $N'P'$, is only on the order of $N\tau/\epsilon T_1$. Since $\tau \sim 1$ μsec and T_1 is typically 10 to 100 sec, for liquid-helium temperatures and for H_0 on the order of a few kOe, it is easy to understand why direct ESR on the RES is doomed to failure, when the pump has only a steady (time-independent) polarization.

E. Steady-State Solution for Pumping with Modulated Polarization ($\tau/T_1' = 0$)

When the (strong) pump light is modulated rapidly and symmetrically between σ^+ and σ^-, then there exists the possibility of obtaining an alternating P' of large amplitude. This result is of fundamental importance to experiments where a large value of P' is needed in conjunction with intense pumping, such as in the search for spin-dependent dichroic effects in the luminescence.[10] It will be assumed here that the polarization is sinusoidally modulated, as in Eq. (3). Thus, $u_+ + u_- = U =$ constant; $u_- - u_+ = u_0 \sin\omega t$; $u_0/U = f$. The most interesting solution is obtained when both limiting conditions $1/T_1 \ll 1/T_p \ll \omega$ are satisfied; the result is then simply

$$P' \cong -\frac{(1-2\epsilon)P_s}{1+(\omega\tau)^2}(\sin\omega t - \omega\tau\cos\omega t) \quad . \tag{18a}$$

According to Eq. (18a), for $1/T_p \ll \omega \ll 1/\tau$, P' will have essentially the full amplitude $(1-2\epsilon)P_s$, and it will be in phase with the pump modulation. Since $1/T_p$ is rarely more than 1000/sec, and since $1/\tau \sim 10^6$/sec, there clearly exists a wide range of modulation frequencies for which one can obtain a large amplitude of P'. Finally, in the limit $\omega\tau \gg 1$, P' will diminish with increasing ω as $1/\omega$, and will asymptotically approach a $\frac{1}{2}\pi$ phase lag with respect to the pumping. In the meantime, for the same conditions as above, that is, for $1/T_1 \ll 1/T_p \ll \omega$, P will remain small:

$$P = \bar{P} + A\sin\omega t + B\cos\omega t \quad , \tag{19}$$

where

$$\bar{P} = \frac{-(T_p/T_1)\tanh\frac{1}{2}\Delta}{1 + T_p/T_1} \quad , \tag{20a}$$

where

$$A = \tfrac{1}{2}\frac{(1-2\epsilon)}{1+(\omega\tau)^2}\, u_0\tau \quad , \tag{20b}$$

and where

$$B = -\frac{1}{1+(\omega\tau)^2}\left(\frac{\epsilon u_0}{\omega}\right) \quad . \tag{20c}$$

Note that $\bar{P} \to 0$ as $T_p/T_1 \to 0$. A behaves as $u_0\tau$, and for the highest differential pump rates obtained in practice, i.e., $u_0 \sim 10^3$/sec, $u_0\tau < 10^{-3}$. Also, for the high modulation frequencies used in the experiments to be described, i.e., $\omega \sim 10^5$/sec, and again for $u_0 \sim 10^3$/sec, $|B| \sim \epsilon u_0/\omega < 10^{-3}$. Finally, we wish to point out the following: In some of the experiments to be described later, the modulated pump beam also serves as the source for a monitor of the MCD of the absorption band. In such an experiment, intensity variations at the detector due to the A and B terms of Eq. (19), will occur only as even harmonics of the modulation frequency, since products such as $\sin^2\omega\tau$ are involved. Thus, the output of the phase-sensitive detector will measure only $\bar{P}$.

F. Steady-State Solution for $\tau/T_1' \neq 0$

Thus far we have treated only the case where the effects of spin-lattice relaxation in the RES are negligible, by setting $\tau/T_1' = 0$ in the equations. Although this represents a very important approximation, valid at sufficiently low temperature, it is also important to consider the more general case, where $\tau/T_1' \neq 0$. For pumping with light of fixed polarization, the steady-state solution for the ground-state polarization P is

$$P = \frac{P_s - (T_p/T_1)\tanh\tfrac{1}{2}\Delta - [\tau/(\tau + 2\epsilon T_1')]\tanh\tfrac{1}{2}\Delta'}{1 + T_p/T_1 - [\tau/(\tau + 2\epsilon T_1')]\tanh\tfrac{1}{2}\Delta'} , \tag{21}$$

where T_p is now given by

$$\frac{1}{T_p} = \frac{\tau + 2\epsilon T_1'}{\tau + T_1'} \frac{u_+ + u_-}{2} , \tag{22}$$

and where the only approximation is that $u_+ + u_- \ll 1/\tau$, i.e., on a time-average basis most of the F centers are in the ground state.

Note that in the limit $\tau/2\epsilon T_1' \gg 1$, $1/T_p \cong \tfrac{1}{2}(u_+ + u_-)$. That is, a sufficiently fast rate $1/T_1'$ will eradicate the spin memory, and hence, in general, much faster pumping rates will be obtained for a given light intensity. This condition may well be fulfilled for temperature $T \sim 10$–$50\,^\circ$K, since it has recently been discovered that T_1' is determined by an Orbach process in that temperature range.[12] For example, in KI, T_1' is presumably on the order of 3×10^6/sec at $T = 20\,^\circ$K. In the meantime, it may be possible to fulfill simultaneously the conditions $\tanh\tfrac{1}{2}\Delta' \ll 1$ and $1/T_1 \ll u_+ + u_-$, even for fields H_0 of several tens of kOe, and for some temperatures in this same range, $T \sim 10$–$50\,^\circ$K. Thus, Eqs. (21) and (22) contain a number of important and positive implications for the operation of an optically pumped maser at temperatures above the liquid-He range.

For saturated pumping with linearly polarized light, i.e., for pumping such that $T_p/T_1 \ll 1$ and such that $P_s = 0$, Eq. (21) simplifies to

$$P = \frac{-[\tau/(\tau + 2\epsilon T_1')]\tanh\tfrac{1}{2}\Delta'}{1 - [\tau/(\tau + 2\epsilon T_1')]\tanh\tfrac{1}{2}\Delta'} . \tag{23}$$

Expression (23) suggests an interesting way to measure T_1', at least in the low-temperature region ($T \lesssim 4\,^\circ$K) where the direct process should be dominant. That is, suppose the crystal is indeed pumped with linearly polarized light of saturating strength. Then the paramagnetic contribution to the MCD signal S_p will just be a measure of the polarization given by expression (23). (The diamagnetic contribution to the MCD signal can always be subtracted out.) Thus, in effect, one can have a measure of the parameter $\tau/2\epsilon T_1'$, at least as long as $\tau/2\epsilon T_1'$ is not too large relative to unity. Since ϵ and τ are already known, T_1' can then be inferred. Such experiments have been performed, and they will be described fully in Sec. VI of this paper. They indicate that spin-lattice relaxation in the RES does indeed have negligible effect on the optical-pumping cycle, for temperatures on the order of 2 °K or less, and at least for H_0 less than 30 kOe.

IV. OPTICAL DETECTION OF ESR IN RELAXED-EXCITED STATE

In this section we wish to show how one may optically detect ESR in the relaxed-excited state by taking proper advantage of the electron-spin memory. The general scheme is as follows: By subjecting the RES to a resonant microwave (ESR) field H_1 while the F center is being pumped with σ^+ or σ^- light, the spin memory can be partially erased, i.e., the resonance will increase the effective value of ϵ. As a consequence, according to Eq. (15b), the *rate* of pumping of the ground-state polarization P is increased. Changes in P thus induced by the resonance in the excited state are measured (and hence the signal is detected) by continuous monitoring of the MCD of the absorption band. Thus, the fundamental detector in these experiments is the ground-state spin system itself.

There are two principal variations on the above scheme. In the first experiments, P was the product of dynamic equilibrium between unsaturated optical pumping and ground-state spin-lattice relaxation. The principal advantage of this "dynamic equilibrium method" is that it provides a most dramatic proof that the resonance in question is indeed that of the relaxed-excited state; otherwise, this method is chiefly of historical interest. The second method uses a pump beam of saturating strength, whose polarization is rapidly and symmetrically modulated between σ^+ and σ^-. It relies on the ability of an H_1 field, resonant with the RES and switched on and off synchronously with the pump modulation, to "rectify" or unbalance the

pumping effects of σ^+ and σ^-. For a number of reasons, this "rectification method" provides superior signal-to-noise ratio. Both methods will be fully described in the following.

For either method, we are interested in the change in the effective value of ϵ, as produced by the resonance in the RES. For the moment, let us suppose that the resonance line in the RES is homogeneously broadened. Then the effects of an H_1 field in exact resonance with the RES can be properly accounted for by adding a term $(-2w_0 n')$ to rate equation (13c), where $w_0 = (\gamma' H_1)^2 \tau$ is the microwave-induced transition rate.[15] (γ' is the electronic gyromagnetic ratio appropriate to the RES.) The solution to the rate equations then yield the following modification of Eq. (15b):

$$\frac{1}{T_p} = \frac{\epsilon + w_0\tau}{1 + 2w_0\tau}(u_+ + u_-) = \epsilon_{\text{eff}}(u_+ + u_-) \quad . \tag{15c}$$

Note that $\epsilon_{\text{eff}} = \frac{1}{2}$ in the limit $w_0\tau \gg 1$; this is a reasonable result, since $\epsilon = \frac{1}{2}$ corresponds to the most complete possible loss of information about the original spin projection. If we define $\delta\epsilon$ by $\delta\epsilon = \epsilon_{\text{eff}} - \epsilon$, then from (15c) we have

$$\delta\epsilon = (1 - 2\epsilon)\frac{w_0\tau}{1 + 2w_0\tau} \quad . \tag{24}$$

Now, in fact, the ESR linewidth in the RES represents an extreme case of inhomogeneous broadening, just as it does in the ground state. Let the inhomogeneous line be described by a shape factor $f(\omega')$, where ω' designates the resonance frequency of a given spin packet, and where

$$\int_{-\infty}^{\infty} f(\omega')\,d\omega' = 1 \quad . \tag{25}$$

Thus, for the inhomogeneous line, we are really interested in the quantity

$$\Delta\epsilon = \int_{-\infty}^{\infty} \delta\epsilon(\omega - \omega') f(\omega')\,d\omega' \quad , \tag{26a}$$

where ω is the actual microwave frequency. For a spin packet of frequency ω', the transition rate is

$$w = w_0/[1 + \tau^2(\omega' - \omega)^2] \quad . \tag{27}$$

By substituting the w of Eq. (27) for w_0 in Eq. (24), we obtain $\delta\epsilon(\omega - \omega')$. Equation (26a) can then be rewritten

$$\Delta\epsilon = \int_{-\infty}^{\infty} \frac{\tau w_0(1 - 2\epsilon)}{2\tau w_0 + 1 + \tau^2(\omega' - \omega)^2} f(\omega')\,d\omega' \quad , \tag{26b}$$

and in the limit $w_0/\tau \ll (\Delta\omega)^2$, where $\Delta\omega$ is the inhomogeneous linewidth, Eq. (26b) becomes

$$\Delta\epsilon = \frac{\pi(1 - 2\epsilon)w_0}{(1 + \tau w_0)^{1/2}} f(\omega) \quad . \tag{28}$$

For the linewidths and highest microwave rates encountered in the experiments to be described, $(\Delta\omega)^2 \gtrsim 10^5 w_0/\tau$. Thus, the approximations leading to Eq. (28) are well satisfied.

For the dynamic equilibrium method, the effects of a resonance can be calculated from

$$\Delta P = \frac{\partial P}{\partial T_p}\frac{\partial T_p}{\partial \epsilon}\Delta\epsilon \quad , \tag{29}$$

where $\Delta\epsilon$ is given by Eq. (28), and where the partial derivatives are to be evaluated from Eqs. (16) and (15b), respectively. Also, when writing the expression for ΔP in its final form, one may substitute T_p/ϵ for $u_+ + u_-$, since $\Delta\epsilon \ll \epsilon$, even for the highest-practical microwave-induced rates w_0. Thus, ΔP is given by

$$\Delta P = \frac{T_p/T_1}{(1 + T_p/T_1)^2}\left(P_s + \tanh\frac{g\mu_B H_0}{2kT}\right)\frac{\pi(1 - 2\epsilon)w_0}{\epsilon(1 + w_0\tau)^{1/2}} f(\omega) \, . \tag{30}$$

Figure 3 shows the apparatus used for the first resonance experiments.[5] A 200-W mercury arc lamp, appropriately filtered, provided a narrow band of wavelengths at one dichroism peak of the absorption band, while a low-intensity narrow band of wavelengths at the other dichroism peak was used for monitoring the MCD. The monitor beam was polarization modulated at 17 kHz, as described in Sec. II, and the pump beam was of a fixed circular polarization. Neutral-density filters in the pump beam allowed control over T_p. Since the microwave-cavity configuration was a bit unusual, it is detailed in Fig. 3(b). The microwave frequencies used were in the neighborhood of 52 GHz; thus both ground-state and excited-state resonances ($g \sim 2$) occurred for H_0 on the order of 20 kOe. Sufficient microwave power was available at the cavity to produce a field $H_1 \sim 1$ Oe; thus $w_0\tau \sim 100$. The samples were electrolytically colored to an F-center concentration on the other of $10^{16}/\text{cm}^3$. After coloration, the samples were mounted into the cavity with the aid of a safe light; from then on they were kept in total darkness until they had been cooled to liquid-He temperatures for the experiment.

Figure 4 shows the behavior of the resonances in KBr for various levels of optical-pumping power. The difference between the line marked $P = 0$ and zero MCD signal is just the diamagnetic signal S_d referred to in Sec. II. By making reference to the thermal-equilibrium signal (obtained with the optical pump turned off), a scale factor for P vs S can be computed, and the grid network $P = -10\%$, etc, added. Note that although the ground-state resonance always points toward $P = 0$, the excited-state resonance always points toward P_s, even when P is inverted; this is in agreement with Eq. (30), which predicts that the sign of ΔP is independent of P for the RES resonance. Thus the origin of the resonance in the RES is well established, as it is very difficult to imagine any

a.

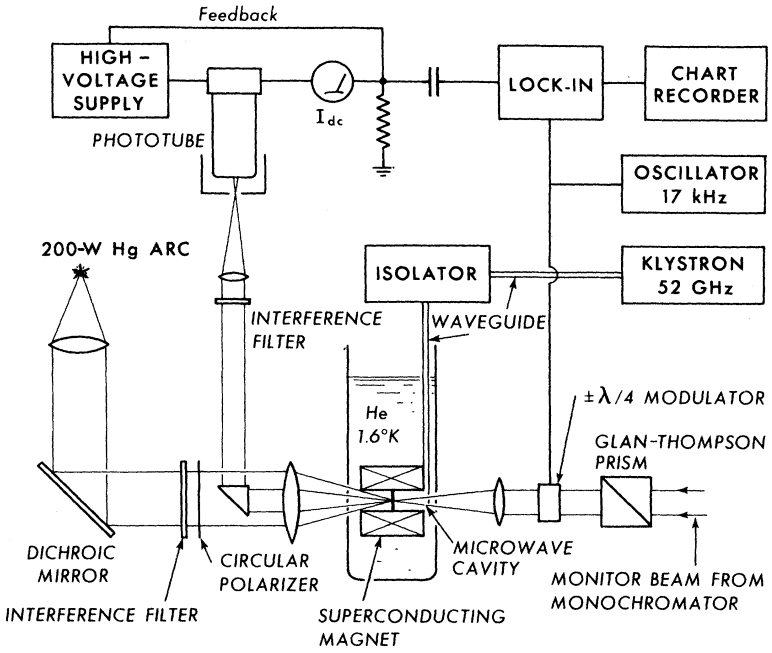

b.

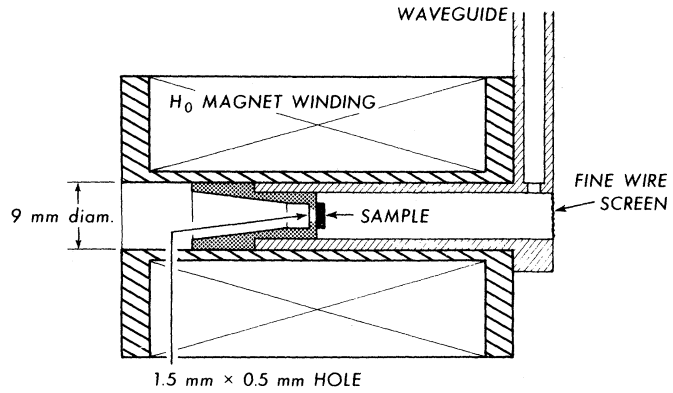

FIG. 3. (a) Block diagram of the apparatus used in the first measurements of ESR in the RES (see text). (b) Detailed view of microwave cavity and superconducting magnet. Monitor-beam cross section at sample was approximately 0.4×0.8 mm; sample thickness ranged from 0.5 to 1 mm. Over this volume of sample, H_0 was constant to within a few Oe in 20 kOe.

other resonance effect that would *increase* P when P is inverted. As a further check, the excited-state resonance signal ΔP, when plotted as a function of the parameter $x/(1+x)^2$, where $x = T_p/T_1$, makes a good fit to a straight line, in conformity with Eq. (30) (see Fig. 5).

The resonance signals in Fig. 4 become distorted as the optical-pumping power is increased, due to a cross-relaxation effect. To understand this effect, one must keep in mind that the MCD signal is sampling the ground-state spin polarization P. There really are two ways by which a microwave field resonant with the RES can affect P: the first is the expected effect predicted by Eq. (30); the second is that the F centers in the RES constitute an "impurity" that can cross relax with the ground state. Since the resonant microwaves raise the RES spin system to a high temperature, the effect of the cross relaxation is always to reduce $|P|$. And since the cross relaxation is strongly dependent on the frequency separation of the interacting centers, the low-field side of the RES resonance affects P more than the high-field side. Thus the low-field side of the signal begins to turn downward at sufficiently high pump levels, while the high-field side continues to point upward. Finally, since the concentration of the cross-relaxing "impurity" increases in direct proportion to the optical-pumping power, while the positive ΔP predicted by Eq. (30) goes to zero at the highest pump levels, the cross-relaxation effect eventually becomes dominant. The effect is much more pronounced in KCl, where the separation between ground-state and RES g factors is much smaller; there the excited-state resonance can be easily and completely inverted at the highest pump levels. In view of the rather high sensitivity of the ESR line shape to the distorting effects of the cross re-

laxation, it is vital to use as high a microwave frequency, and as low an F-center concentration, as possible. Thus, the fact that only low F-center concentrations are required for optical detection of resonance, has yielded yet another (even if somewhat unexpected) advantage to that technique.

Although no careful quantitative check has yet been made, the resonance signals seem to show the dependence on ϵ and ESR linewidth predicted by Eq. (30). In this regard, the comparison of KI to KBr is most dramatic: Whereas the signals in KBr are rather large, as shown in Fig. 4, the corresponding signals in KI are roughly an order of magnitude smaller; this reflects the nearly five times increase in ϵ, as well as the approximately twofold increase in resonance linewidth of KI with respect to KBr.

In view of the small size of the ESR signals in KI, and of the need for higher sensitivity if the optical detection is to be used for the observation of ENDOR in the RES, it would be highly desirable to have a true lock-in detection on the ESR or ENDOR itself. In the dynamic equilibrium method, with the optical-pumping intensity adjusted to give optimum sensitivity, P can change at a rate no greater than $\sim 2/T_1$ in response to the application of H_1 fields resonant with the RES. [According to Eq. (30), optimum sensitivity occurs at $T_p/T_1 = 1$.] Since T_1 is of the order of seconds, the resultant slow "detector" response time mitigates against the use of the desired lock-in detection.

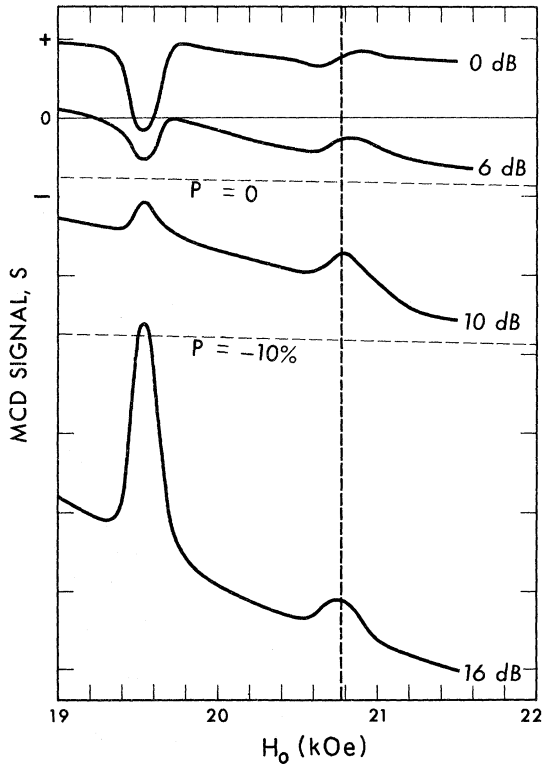

FIG. 4. MCD signal vs H_0 for various optical-pump powers, for detection of ESR by the dynamic-equilibrium method. Light-pump-power attenuation indicated in dB. Ground-state resonance is at the left-hand side. Dashed vertical line shows center of the excited-state resonance; cross relaxation distorts the line shape at high pump powers (see text).

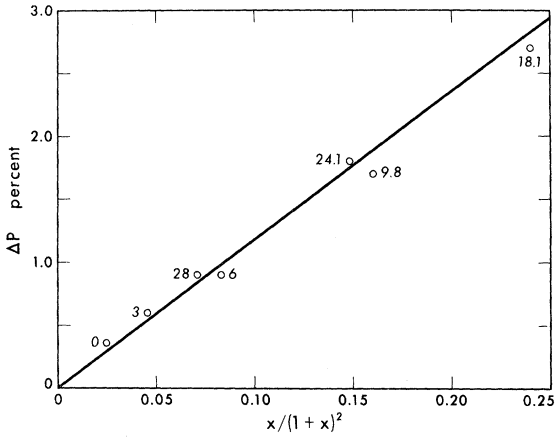

FIG. 5. Excited-state-resonance signal ΔP, plotted as a function of the parameter $x/(1+x)^2$, where $x = T_p/T_1$. Open circles are the experimental points; the number beside them indicate the relative pump-power attenuation in dB. The straight line represents the best fit.

The rectification method was invented to circumvent the above-mentioned limitation. It uses a very intense optical-pumping beam to produce a detector response time T_r orders of magnitude faster than T_1 [see Eq. (15a)]. The method is best understood through reference to Fig. 6. The intense pump beam is switched rapidly and symmetrically between σ^+ and σ^- polarization. (The actual light-modulation frequencies used in the latest experiments have been 50 and 9.1 kHz.) In the absence of resonance effects in the RES, the resultant ground-state polarization P will be essentially zero [see Eqs. (19) and (20)]. But suppose microwaves resonant with the RES are switched on and off synchronously with the polarization, such that the H_1 field coincides in time with, say, σ^+. Then the pumping effect of σ^+ on P will be greater than that of σ^-, and P will rise to a new equilibrium value given by

$$P \cong P_s \frac{\Delta\epsilon}{2\epsilon} \quad , \tag{31}$$

where P_s and $\Delta\epsilon$ have been defined by Eqs. (10) and (28), respectively. P will reach essentially the full value given by (31) in an interval just several times T_r. Then, by reversing the relative phase of the light modulation and the H_1 switching, the sign of P can be reversed. In this way, one

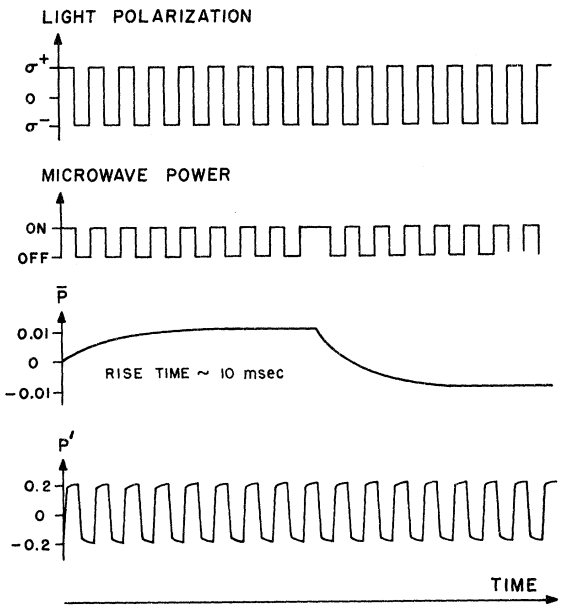

FIG. 6. Relative time dependencies of the pump-light polarization, microwave power, ground-state polarization $\bar{P}$, and excited-state polarization P', for detection of ESR in the relaxed-excited state by the rectification method (see text).

can generate, at the phase-switching frequency, an ac voltage containing only the resonance signal. Since rates $1/T_r > 100/\text{sec}$ can be achieved in practice, the phase-switching or second lock-in frequency can be on the order of 10 Hz.

Equation (31) was derived as follows: If one sets $P_i = P$ and $P_f = P_s$ in the time derivative of Eq. (14), then the rates at time $t = 0$ are

$$\frac{dP}{dt} = (P_s - P)(\epsilon + \Delta\epsilon)(u_+ + u_-) \ , \tag{32a}$$

for pumping with σ^+, and

$$\frac{dP}{dt} = (-P_s - P)\epsilon(u_+ + u_-) \ , \tag{32b}$$

for pumping with σ^-, assuming that H_1 is coincident with σ^+. The rates given by Eqs. (32a) and (32b) must sum to zero if the time-average value of P is to remain steady. Equation (31) then follows almost immediately.

The rectification method has the further advantage that the signal will be highly insensitive to changes in the crystal-lattice temperature. That is, the spin polarizations in both the ground and relaxed-excited states are determined almost entirely by the fast optical-pumping and resonance effects; hence, the relatively slow spin-lattice-relaxation processes are almost completely overwhelmed. This insensitivity to lattice temperature is especially important in the extension of the method to include ENDOR, since in the process of generating large rf fields for the ENDOR, much heat is dissipated in the immediate neighborhood of the sample. The ENDOR will be fully described in the next section.

The rectification method was given its first experimental test on the ESR in KBr and KI.[6] The latest version of the apparatus used is shown in Fig. 7. The H_0 field of ~ 22 kOe was supplied by a split-coil superconducting magnet of modest size. Both crystal and magnet shared the same He bath at 1.6 °K. The crystal samples (1 mm^2 $\times$ 0.6 mm thick, $< 10^{17} F$ centers/cm^3) were mounted inside a 4-mm-thick$\times$ 7-mm-diam microwave cavity. The cavity operated in the TM_{110}. It had a pair of ~ 0.5-mm-diam holes on its axis to allow for passage of light. Both crystal [100] axis and the pump-light beam were parallel to H_0. A single He-Ne laser beam at 6328 Å functioned as both pump and MCD monitor. (Figure 1 shows how 6328 Å relates to the absorption bands in KBr and KI.) Actual pump power available at the crystal was about 3 to 5 mW, focused onto a spot of about 200-μm diam. The polarization was modulated at 9.1 kHz by an oscillating $\pm\frac{1}{4}\lambda$ plate of fused silica before it impinged on the sample. The transmitted light created an MCD signal at the phototube as explained in Sec. II. After processing by a lock-in detector at 9.1 kHz

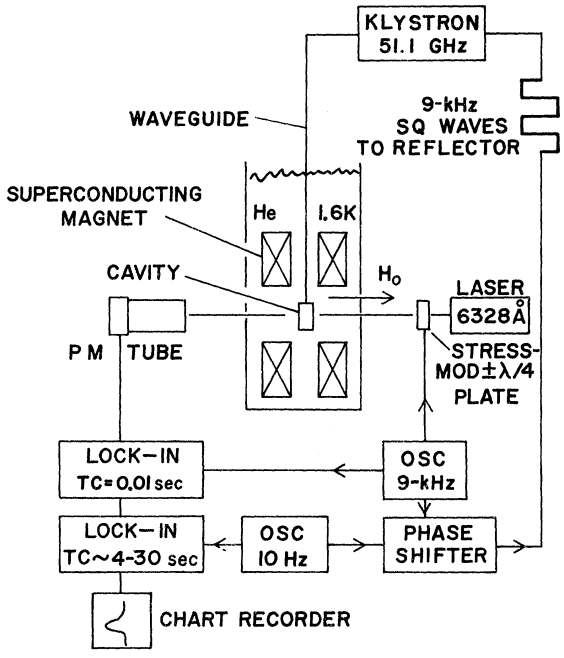

FIG. 7. Block diagram of the apparatus used for detection of ESR in the relaxed-excited state by the rectification method. TC is lock-in integration time constant (see text).

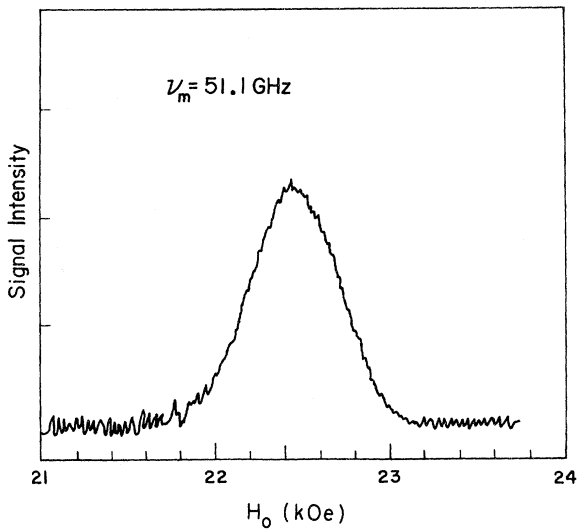

FIG. 8. ESR signal due to resonance in the RES in KI, as obtained by the rectification method. ν_m is the microwave frequency.

(integration time 0.01 sec), the MCD signal was sent through a second lock-in at 10 Hz. A 9.1-kHz reference voltage from the light modulator was phase reversed at 10 Hz before it was made into a square wave for turning the H_1 field on and off.

By applying the 9.1-kHz square waves to the klystron reflector, the microwave frequency ν_m could be switched in and out of resonance with the cavity (cavity $Q \sim 5000$). Hence, the H_1 field seen by the sample was very effectively turned on and off. Sufficient microwave power was available at the cavity to allow $H_1 \sim 1$ Oe. The ESR signal due to the RES in KI is shown in Fig. 8. It represents a vast improvement in signal-to-noise ratio over that obtained for KI by the dynamic-equilibrium method.

Table I summarizes the ESR data for the F-center RES in KCl, KBr, and KI, as obtained in this laboratory.[5,6] Linewidths and g factors for the ground-state resonance are included for easy comparison; the numbers are from a review article by Seidel and Wolf.[16] The linewidths are always given here as the full width at half-intensity points. The RES g factors listed are isotropic within the limits of experimental error, although the question of isotropy has not yet been given a thorough check; to date only the KCl g factor has been measured for the H_0 field along the [100], [110], and [111] axes; the others have been measured only for H_0 parallel to [100]. However, there now exists a new piece of evidence in favor of isotropy: recently, the Neuchâtel group[12] have detected the RES resonances at nearly one-order-of-magnitude smaller field H_0, and they obtain essentially the same linewidths for KBr and KI as in our measurements. Nevertheless, the orientation dependence of the RES g factors and linewidths should be given a very careful and thorough check at the highest possible fields H_0, where cross-relaxation effects and problems of resolving the ground-state and RES resonances are insignificant.

A complete theoretical analysis of the RES g factor is beyond the scope of this paper, especially in view of the fact that no truly viable theory of the RES exists to date. However, certain general observations can be made. First, if it can be assumed that the "spin-up" and "spin-down" sublevels of the RES are time-reversal symmetric with respect to each other, then the g factor is just given by

$$g = 2\left(\frac{m}{m^*}\langle L_z\rangle + 2\langle S_z\rangle\right) , \tag{33}$$

where $\langle L_z\rangle$ and $\langle S_z\rangle$ refer to the "spin-up" state, and where m/m^* represents the ratio of ordinary to effective electron mass. The ratio of m/m^* must be included, to account for the possibility that the RES is spatially diffuse. That is, the concept of effective mass would be meaningful for a truly diffuse state, and in general, one would have $m/m^* \neq 1$.

According to the ideas presented in the following paper, on a time-average basis, even at $T = 0$, the zero-point lattice vibrations produce rather large noncubic fields at the F-center site. These noncubic fields tend to quench the orbital momentum of p states. If the energy splittings associated with the noncubic field are characterized by a parameter D, while the spin-orbit energy is characterized by a parameter λ, then in the limit $\lambda \ll D$, the $\langle L_z\rangle$ is of order λ/D, while the degree of spin mixing is only of order $(\lambda/D)^2$.

The analysis referred to above is based on the adiabatic approximation, and it is valid primarily for the calculation of optical-transition probabilities into the absorption band; even then, the requirements of the adiabatic approximation are not always satisfied. Nevertheless, it is not unreasonable to suppose that the $\langle L_z\rangle$ and the degree of spin mixing are related to each other in the RES more or less as indicated above. If that is true, then the degree of spin mixing in the RES, ϵ_3, is rather small (as we have already asserted in Sec.

TABLE I. Summary of ESR data.

Host crystal	Relaxed-excited state g factor	Relaxed-excited state ΔH, width at half-power points (Oe)	Ground state g factor	Ground state ΔH, width at half-power points (Oe)
KCl	1.976 ± 0.001	55 ± 2	1.995	55
KBr	1.862 ± 0.002	270 ± 10	1.982	146
KI	1.627 ± 0.002	575 ± 20	1.964	263

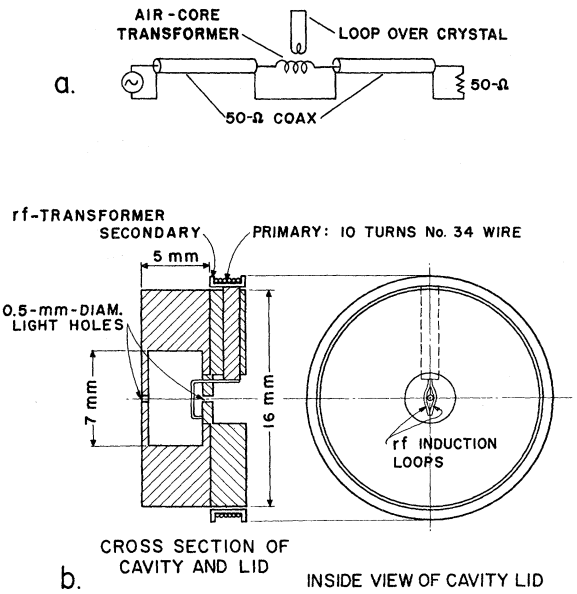

FIG. 9. (a) Schematic diagram of the arrangement for producing large rf H_{11} fields at the sample. The generator and 50-Ω load are both outside the Dewar; the transformer is inside the Dewar, near the sample. The arrangement has a bandpass in excess of 100 MHz (see text). (b) Details of the microwave cavity. The rf transformer and induction loop are the same as those indicated schematically, above in (a).

II), and the $\langle S_z \rangle$ can be set $\simeq \frac{1}{2}$ for substitution into Eq. (29). Thus the large shifts of g from $g = 2$ must be accounted for primarily by the term $(m/m^*)\langle L_z \rangle$, and, unless m^* is unusually small, a rather large absolute value of $\langle L_z \rangle$ itself is implied.

According to the above, the g shift should give us information about the ratio λ/D. Now, it is not unreasonable to imagine that the effective value of D would diminish rather rapidly as the mean radial extent of the RES wave function were increased. If the theoretical dependence of λ on the radial extent of the RES were also known, it might be possible to speculate on the "diffuse" vs "compact" nature of the RES on the basis of the measured g factors alone. At least the rapid increase in the g shift with increasing halide weight is consistent with the above ideas; it has been well established that λ in the absorption band increases rapidly as one goes from KCl to KI.

However, the sign of the g shift presents a problem. That is, according to the wave functions given in the following paper, a shift $g-2<0$ corresponds to $\lambda/m^*>0$ for the lowest-lying magnetic doublet. Since $\lambda<0$ in the absorption band, one must either invoke a negative m^*, or else believe that in the RES λ has the opposite sign from its value in the band.

V. OPTICAL DETECTION OF ENDOR IN RELAXED-EXCITED STATE

The optical-detection techniques of the previous section can be extended to include ENDOR of the RES. The extension is based on the following general principles: As indicated previously, the microwave H_1 field can be made strong enough to at least partially saturate a single spin packet out of the total ESR linewidth. Thus, nuclear-spin flips due to an rf H_{11} field will have the net effect of bringing more spin packets into resonance with the microwaves, and hence the microwave effect on the optical pumping will be augmented. In practice, the actual size of the ENDOR effect is surprisingly large; that is, the ENDOR signals are often as strong as the ESR itself. Thus, when the rectification method is employed for the detection of ENDOR, obtaining a good signal-to-noise ratio is no longer a problem.

The most difficult and fundamental problems result from the short optical decay time τ of the RES. For the host lattices KCl, KBr, and KI, one has $\tau = 0.5, 1.1$, and 3 μsec, respectively, at liquid-He temperatures.[17,18] In the first place, these short lifetimes limit the minimum-resolvable ENDOR frequency difference, $\Delta\nu_{11}$, to $\Delta\nu_{11} \sim (\pi\tau)^{-1}$, or $\Delta\nu_{11} \sim 0.4$ MHz for $\tau \sim 1$ μsec. Since the most important ENDOR frequencies are spread out over a region of several tens of MHz, the lifetime-limited resolution does not always pose as serious a problem as might appear at first thought. A somewhat greater practical difficulty arises from the following: In order to bring the ENDOR signal close to its saturated value, the condition

$$(\gamma_n H_{11}\tau)^2 \gtrsim 1 \tag{34}$$

must be satisfied, where the gyromagnetic ratio γ_n refers to the nuclei interacting with the F center, and where H_{11} is the amplitude of the rf ENDOR field. Although γ_n is really an effective value whose size can be augmented by the hyperfine coupling itself,[19] nevertheless the required value of H_{11} computed from Eq. (34) is usually on the order of 100 Oe or more. Since ν_{11} must be scanned over a very wide frequency range, the generation of such H_{11} fields poses a severe technological challenge. We have been able to overcome this problem, primarily by taking advantage of the very small sample size required for optical detection.

The arrangement for producing large rf H_{11} fields is shown schematically in Fig. 9(a). Current from an rf power oscillator was sent through a 50-Ω coaxial cable to a 50-Ω load located outside the Dewar. On its way, the current passed through the primary of a tightly coupled air-core current transformer located near the sample. Thus magnified 10 times, the current was sent through a

single-turn wire loop which passed around the sample inside the microwave cavity. Since the loop enclosed less than 1-mm^2 area, a primary current of 1 A was able to produce H_{11} fields at the sample of about 100 Oe, as verified by direct measurement of the voltage induced in a tiny pickup loop of known dimensions. The same measurements showed H_{11} to be a constant with respect to ν_{11}, as long as the voltage at the 50-Ω load was held constant. The measurements were made over the range $10 \leq H_{11} \leq 100$ MHz. In the latest experiments, the voltage at the 50-Ω load was held precisely constant by a negative-feedback loop that acted to control the oscillator output power. Finally, it should be pointed out that the distributed capacity between the rf-transformer primary and secondary plays an important role; since the secondary acts as a ground plane, the primary can be made to look like a section of 50-Ω transmission line. The capacity was adjusted to the correct value by putting polystyrene "Q dope" between the primary and secondary, and by choosing the proper wire gauge for the primary. By this means, the standing-wave ratio in the circuit of Fig. 9(a) was held very close to unity, even for frequencies well in excess of 100 MHz.

The modified microwave cavity is shown in Fig. 9(b). It is essentially the same as the cavity described in Sec. IV for use with the detection of ESR by the rectification method, except for the addition here of the rf transformer, wound around its outer perimeter, and the tiny rf induction loop inside. Note that the induction loop is split in two, in order to make that H_{11} field component which is parallel to H_0 as small as possible. This is to avoid an annoying, more-or-less frequency-independent background effect due to a sufficiently rapid modulation of H_0 ($\nu_{11} > 1/\tau$); such a modulation will also augment the number of spin packets affected by the H_1 field. Note further that one of the cavity faces is parted (to allow for insertion of samples) at a radius where the surface currents are precisely circular; thus cavity Q is preserved without the need for electrical conduction across the parting circumference.

The size of the ENDOR signals ought to increase monotonically with increasing depth of the hole "burned" into the ESR line by the microwaves. Furthermore, for an H_1 field of saturating strength, the hole depth ought to be just equal to the magnitude of P' itself. Thus it is important to maximize the amplitude of P', and to make the phase shift between P' and the light switching small relative to $\frac{1}{2}\pi$. For that reason, in the latest ENDOR experiments, the light-modulation frequency was lowered from 50 to 9.1 kHz. Equation (18a) implies that the phase shift in question will be given by

$$\theta = \tan^{-1}(\omega\tau) \quad . \tag{18b}$$

For KI, $\tau = 3$ μsec and $\theta \sim 45°$ when $\omega/2\pi = 50$ kHz, whereas it is reduced to the essentially negligible value of $\theta \sim 10°$ when $\omega/2\pi = 9.1$ kHz.

Except for the addition of the rf gear described above, the apparatus is essentially the same as that illustrated in Fig. 7 and described in Sec. IV. The only other change is that the square waves at the light-modulation frequency are now used to turn the rf power on and off, and the microwaves are *not* modulated. In this way the modulation at the 10-Hz phase-reversal frequency corresponds to the ENDOR effect alone.

Figure 10 shows the best ENDOR spectrum obtained to date for the F center in KI. H_0 was tuned to the ESR line center of the RES ($H_0 = 21.72$ kOe). At least 12 highly repeatable features are to be

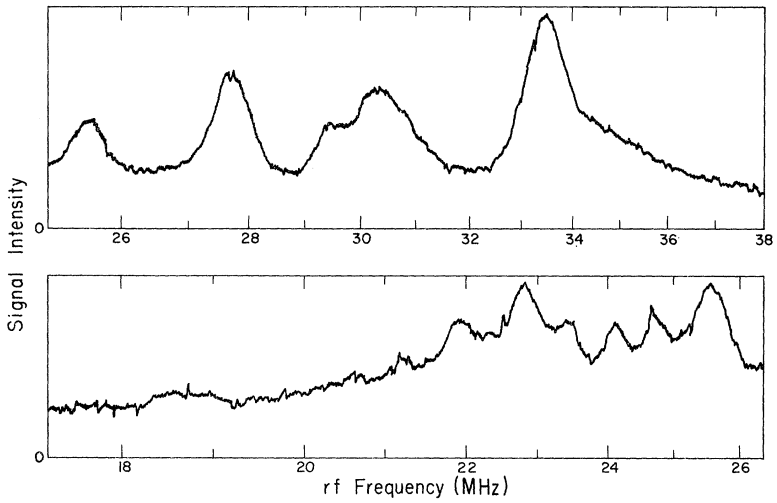

FIG. 10. ENDOR spectrum of the RES in KI. $H_0 = 21.72$ kOe. Amplitude of the H_{11} field was somewhat larger for the lower curve (see text).

seen in the region $20 \lesssim \nu_{11} \lesssim 35$ MHz. No resolved peaks have been seen for $\nu_{11} \lesssim 20$ MHz, and there is essentially no response at all for $\nu_{11} \gtrsim 38$ MHz, save for a small frequency-independent background effect. The latter is probably just due to the modulation of H_0 by H_{11}, as described earlier. (In our first report[6] on the ENDOR in the RES, we indicated that there was some evidence for "signals" in the neighborhood of 70 MHz; these have since turned out to be an entirely spurious effect.) By comparing the results of Fig. 10 with those of our earlier work, taken at slightly higher field (H_0 = 22.45 kOe), the five or six highest-frequency ENDOR lines are seen to shift toward higher frequency with increasing H_0, and by the proper amount for I^{127} nuclei. Since the nuclear Zeeman frequency, $\nu_z \sim 19$ MHz for I^{127} and for $H_0 \sim 22$ kOe, the ENDOR lines in question must represent sum frequencies, i.e., $\nu_{11} = \nu_z + \nu_{hf}$, where ν_{hf} is the frequency associated with the hyperfine-interaction energy. Thus the ν_{hf} values for I^{127} would appear to be spread out more or less uniformly over the range $0 < \nu_{hf} < 15$ MHz. This is somewhat in contrast to the ground state in KI, where for iodine nuclei, $\nu_{hf} \sim 20$ MHz for the closest shell, and where the frequencies associated with all other shells are smaller by an order of magnitude or more.[20] In fact, for the ground state in KI, over 90% of the ESR linewidth can be accounted for by the almost isotropic interaction with the 12 nuclei of the closest iodine shell.

VI. MEASUREMENT OF T_1'

In Sec. III F of this paper, we briefly described a purely optical technique for the measurement of the spin-lattice relaxation time T_1' in the RES. The method is based on the fact that for truly saturated pumping with linearly polarized light, the resultant ground-state polarization P should differ from zero only because of spin-lattice relaxation, while the F centers are in the RES. Equation (23) gives an expression for P under the above conditions. A measurement of P by the MCD of the absorption band should then give rather direct information about T_1'.

In practice, there are two problems: The first is to separate out the usually rather small paramagnetic signal S_p, resulting from the P of Eq. (23), from the diamagnetic term S_d. This separation may be accomplished by taking advantage of the different field dependencies of the two terms in the MCD signal. That is, at sufficiently low temperature, say $T \lesssim 2K$, $1/T_1'$ ought to result exclusively from a direct process. Thus it will have a field dependence[3] of the well-known form

$$1/T_1' = AH_0^3 \coth\tfrac{1}{2}\Delta' \ . \tag{35}$$

By combining Eqs. (35) and (23), it can be seen that S_p, considered as a function of H_0, will have zero slope at $H_0 = 0$. In the meantime, S_d is directly proportional to H_0. Thus the tangent to the experimentally measured curve of $S(H_0)$ at $H_0 = 0$ ought to give $S_d(H_0)$. Of course, S_d can also be determined by measuring $S(H_0)$ at two different lattice temperatures.

The second problem is that it is not always easy to produce sufficiently saturated pumping, such that the effects of ground-state relaxation are made completely negligible relative to the contribution of Eq. (23). To examine this point in greater detail, let us consider the general result given by Eq. (21) once again. If $P_s = 0$, and T_p/T_1 and $\tau/2\epsilon T_1'$ are each small relative to unity, then Eq. (21) may be written

$$P \cong -(T_p/T_1)\tanh\tfrac{1}{2}\Delta - [\tau/(\tau + 2\epsilon T_1')]\tanh\tfrac{1}{2}\Delta' \ . \tag{36}$$

Thus, to make the second term dominant, we require that $(2\epsilon T_p/\tau)(T_1'/T_1) \ll 1$, or equivalently, we require that $T_1' \ll (u\tau)T_1$. Since it is difficult in practice to make the fraction $u\tau$ much bigger than about 10^{-3} or at most 10^{-2}, the maximum T_1' that can be measured with this technique is on the order of $10^{-3}T_1$.

The apparatus used for the T_1' measurements is shown in Fig. 11. The beam of a 5-mW He-Ne laser was focused onto the sample, such that the diffraction-limited spot size was on the order of 50 μm in diameter. Thus the pump intensity was on the order of several hundred W/cm^2. The same beam was also used to monitor the MCD, and therefore it was polarization modulated at 50 kHz. An adjustable birefringence plate was used in addition

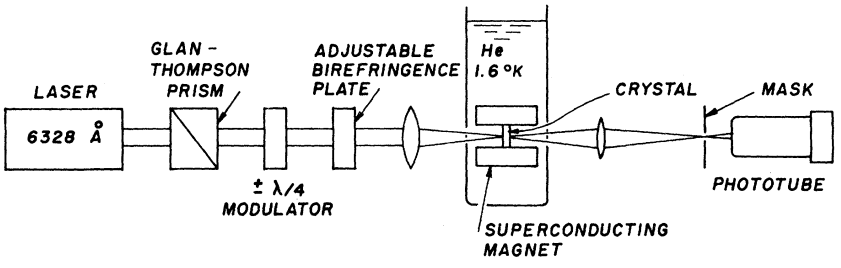

FIG. 11. Block diagram of the apparatus used for T_1' measurements (see text).

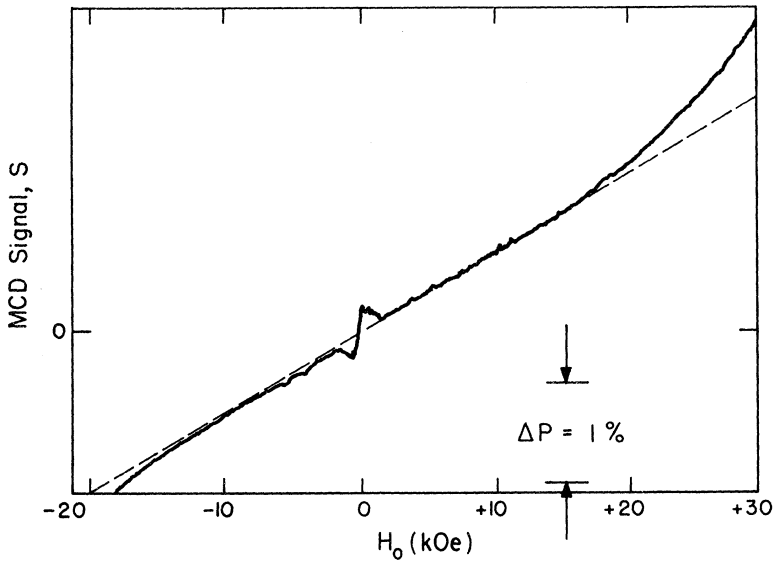

FIG. 12. MCD signal as a function of magnetic field for very fast pumping with light whose polarization is linear on a time-average basis. Presumably the dashed line represents the diamagnetic signal S_d. The difference between the measured curve (solid line) and the dashed line then represents the ground-state polarization resulting from $1/T_1'$ (see text). Origin of the kink in the neighborhood of $H_0=0$ is not known, but it may be due to cross-relaxation effects.

to the modulator, to adjust the modulation to precise symmetry about linear polarization. As pointed out in Sec. III E the lock-in detector is not sensitive to the component of P oscillating at 50 kHz. Thus, for the purposes of this experiment, the modulated beam is equivalent to a linearly polarized one.

The results of a measurement at $T=1.6\,^{\circ}\mathrm{K}$ on the F center in KI are shown in Fig. 12. The vertical scale was calibrated in terms of percent polarization by making reference to the signal produced by a thermal-equilibrium polarization. Owing to the poor quality of the sample surfaces, there was a rather strong halo of scattered light surrounding the bright central spot on the sample. Since this halo only weakly pumps those parts of the crystal it passes through, it contains a large paramagnetic signal. It should be possible to avoid the effects of this halo on the signal by carefully imaging the crystal sample onto the phototube surface, and by masking off the image of the halo. Unfortunately, in the experiment whose result is shown in Fig. 12, the hole of the mask was too large. Thus, most of the deviation of the curve of Fig. 11 from a straight line is probably due to terms like the first of Eq. (36). Nevertheless, the experiment does serve to put an upper bound on $1/T_1'$. For example, at $H_0=30$ kOe and at $T=1.6\,^{\circ}\mathrm{K}$, we obtain $1/T_1' \lesssim 1500/\mathrm{sec}$. Thus, even with this imperfect result, it can be seen easily that the effects on the optical pumping of spin-lattice relaxation in the RES are negligible at $1.6\,^{\circ}\mathrm{K}$.

An improved arrangement for these measurements of T_1' is in preparation. With it, it should be possible to measure T_1' over a wide range of temperatures as well as field.

Note added in proof. Recently, Mollenauer and Baldacchini have calculated both the ESR linewidth ΔH and the ENDOR frequencies ν_{hf} for the RES in KI, on the assumption of a pure $2p$ wave function of the form $\psi = A\rho e^{-\eta\rho}\cos\theta$, where ρ is the radial distance measured in units of the lattice spacing, and where the angle θ is measured from a [100] axis. They obtain an excellent fit to both ΔH and the largest values of ν_{hf}, for a value of the parameter $\eta = 0.33$ (for $\eta \lesssim 1$, the calculated ΔH increases as $\eta^{3/2}$; thus η is sharply defined by ΔH as well as by the individual ν_{hf}). Thus a very diffuse wave function is implied, in good agreement with the predictions of Fowler's theory.[21] Furthermore, essentially the same value of η correctly predicts the measured ΔH values for the RES in KBr and KCl. The question of admixture of $2s$ into the RES wave function is also being considered, but preliminary results indicate that such admixture will not radically alter the mean radial extent of the wave function. Details of the calculation will be submitted for publication elsewhere.

Recent measurements of the angular dependence of the ENDOR frequencies in KI are also consistent with the above. That is, there are no measurable shifts when the crystal axes are rotated with respect to the magnetic field direction. It should be remembered that the anisotropies in the hyperfine interaction arise from ordinary dipole-dipole terms, and that these become very small for a highly diffuse electronic state.

Finally, rotation of the crystal axes with respect to the magnetic field direction produces no measurable change in either the g factor or ΔH for the RES in KI. Thus the g factor is indeed isotropic for the RES, and ΔH must be explained entirely in terms of unresolved hyperfine splittings.

ACKNOWLEDGMENTS

First, we would like to extend the most profound thanks to Professor C. D. Jeffries for his constant encouragement and support of this work. We also gratefully acknowledge the assistance, at various times in the experiments, of S. Yngvesson, A. Winnacker, and G. Baldacchini. And a few of the many other individuals with whom we have had fruitful discussions are W. B. Fowler, S. Geschwind, J. Margerie, Y. Merle D'Aubigne, D. Schmid, and H. Seidel.

*Research supported in part by the U. S. Atomic Energy Commission, Report No. UCB-34P20-149.

[1]N. V. Karlov, J. Margerie, and Y. Merle-D'Aubigne, J. Phys. (Paris) 24, 717 (1963).

[2]J. Mort, F. Lüty, and F. C. Brown, Phys. Rev. 137, A566 (1965).

[3]H. Panepucci and L. F. Mollenauer, Phys. Rev. 178, 589 (1969).

[4]D. Schmid and V. Zimmerman, Phys. Letters 27A, 459 (1968).

[5]L. F. Mollenauer, S. Pan, and S. Yngvesson, Phys. Rev. Letters 23, 689 (1969).

[6]L. F. Mollenauer, S. Pan, and A. Winnacker, Phys. Rev. Letters 26, 1643 (1971).

[7]W. B. Fowler, in *Physics of Color Centers*, edited by W. B. Fowler (Academic, New York, 1968).

[8]M. P. Fontana and D. B. Fitchen, Phys. Rev. Letters 23, 1497 (1969).

[9]M. P. Fontana, Phys. Rev. B 2, 4304 (1970).

[10]L. F. Mollenauer and G. Baldscchini (unpublished).

[11]F. Porret and F. Lüty, Phys. Rev. Letters 26, 843 (1971).

[12]Y. Ruedin, P. A. Schnegg, M. A. Aegerter, and C. Jaccard, Proceeding of 1971 International Conference on Colour Centres in Ionic Crystals at Reading, England, 1971 (unpublished), see abstracts 48 and 49.

[13]K. H. Becker and H. Pick, Nachr. Akad. Wiss. Göttingen, II Math-Physik K1, 167, (1956).

[14]M. P. Fontana [Phys. Rev. B 2, 4304 (1970)] has made the assumption that $P' = \pm P_s$ for saturated pumping with σ^+ or σ^- light, whereas we have shown here that $P' = 0$ under those conditions. Therefore, his conclusion that spin-dependent polarization effects in the luminescence are immeasurably small is based on a false premise. This has also been shown recently by Baldacchini (see Ref. 10). Thus, Fontana's conclusion about λ in the RES is also groundless.

[15]See any standard text on the resonance phenomenon. Here τ plays the role of T_2.

[16]H. Seidel and H. C. Wolf, in *Physics of Color Centers*, edited by W. B. Fowler (Academic, New York, 1968), p. 555.

[17]H. Mahr, in Ref. 16, p. 270.

[18]Reference 16, Appendix B, p. 627.

[19]Abragam and Bleaney, *Electron Paramagnetic Resonance of Transition Ions* (Clarendon, Oxford, 1970), pp. 221–222.

[20]H. Seidel, Z. Physik 165, 218 (1961).

[21]W. B. Fowler, in Ref. 16.

PHYSICAL REVIEW B VOLUME 6, NUMBER 3 1 AUGUST 1972

Spin Mixing and Magnetic Circular Dichroism in the Absorption Band of *F* Centers–A Theoretical Investigation of Electron-Spin Memory*

A. Winnacker† and L. F. Mollenauer
Department of Physics, University of California, Berkeley, California 94720
(Received 14 February 1972)

A theoretical model of the *F*-center absorption band is described. From it are calculated both the magnetic circular dichroism (MCD) and the spin mixing in the optical-pumping cycle. Despite the fact that it is based on the sometimes doubtful adiabatic approximation, in general, agreement with experiment is good. In particular, it shows that a moderately large MCD effect will be accompanied by a relatively small degree of spin mixing.

I. INTRODUCTION

In this paper two interrelated phenomena, associated with the optical pumping of *F* centers in alkali halides, are investigated from a theoretical point of view: the spin memory, and the magnetic circular dichroism (MCD) of the absorption band. These two phenomena have been discussed in length phenomenologically and experimentally in the foregoing work,[1] henceforth referred to as I. Therefore, we shall recapitulate here only those facts and definitions that are required to make this paper self-contained. For all details of experimental observation and exploitation of these effects, the reader is referred to I.

The MCD of the *F* absorption band in alkali halides is rather large.[2,3] That is, for right- or left-circularly polarized light propagating along the externally applied field H_0 (σ^+ and σ^- transitions), the fraction $f = (\alpha^+ - \alpha^-)/(\alpha^+ + \alpha^-)$, where